Chinese Chemical Letters 32 (2021) 1507–1510

Contents lists available at ScienceDirect

Chinese Chemical Letters

journal homepage: www.elsevier.com/locate/cclet

Communication

Facile synthesis of ternary $AgInS_2$ nanowires and their self-assembly of fingerprint-like nanostructures

Jing Zhang[a], Bin Zeng[a], Haihang Ye[c,**], Aiwei Tang[a,b,*]

[a] Department of Chemistry, School of Science, Beijing JiaoTong University, Beijing 100044, China
[b] Key Laboratory of Luminescence and Optical Information, Ministry of Education, School of Science, Beijing JiaoTong University, Beijing 100044, China
[c] Mechanical Engineering Department, University of Texas at Dallas, Richardson, TX 75080, United States

ARTICLE INFO

Article history:
Received 8 August 2020
Received in revised form 26 September 2020
Accepted 28 September 2020
Available online 29 September 2020

Keywords:
$AgInS_2$ nanowires
Self-assembly
Fingerprint-like structure
Seeded-mediated growth
Semiconductor nanocrystals

ABSTRACT

Nanowires (NWs) and self-assemble nanostructures made of chalcogenide semiconductor nanocrystals (NCs) are of great interests to the fundamental studies and practical applications. In this study, we reported a seeded-mediated growth of $AgInS_2$ NWs and their intriguing self-assembly nanostructures with fingerprint-like shape. The key to the formation and self-assembly of $AgInS_2$ NWs was the presence of In-S species that was a type of molecular metal chalcogenide complexes, serving as specific inorganic ligands for the growth of NWs and cross-linker molecules for the self-assembly of fingerprint-like nanostructures. Systematic studies were carried out to investigate the reaction factors, including the thermodynamics, amount and type of In precursors, and 1-dodecanethiol usage, to the success of the desired products.

Chalcogenide semiconductor nanocrystals (NCs) made of $AgInS_2$ have received great attention in recent years due to their unique band gap structures and optical properties, serving as promising alternatives for the more toxic cadmium-based NCs [1–3]. These features make them good candidates in many applications including solar cells [4–6], light-emitting diodes [7–11], biological labels [12–16], photocatalysis [17,18] and so on [19,20]. Therefore, the controllable synthesis of $AgInS_2$ NCs in terms of their shape, size, and phase structure is of fundamental and practical importance since their properties are highly dependent on the physical parameters [21–23].

Among variety shapes of NCs, nanowires (NWs) represent for typically one-dimensional nanostructures with the confined geometry and large number of exposed atoms on surface, which are mainly responsible for their enhanced properties and superior performance. For example, wurtzite $CuInS_2$ NWs were reported with enhanced photoresponsivity [24]. However, due to the presence of Cu_2S NCs as catalysts for the growth of the $CuInS_2$ NWs, the products are often inhomogeneous [24,25]. Therefore, it remains challenging to produce ternary semiconductor NWs with high purity and uniformity. In addition, self-assembly of semiconductor NCs paves a simple yet cost-effective way for the further design and construction of NCs superlattices, which sets the basis of nanodevices fabrication [26–28]. For example, Taniguchi *et al.* proposed a simple route to the end-to-end self-assembly of CdSe nanorods through ligand exchange with short-chained water-soluble thiols [29]. However, the additional step of ligand exchange adds complexity to the preparation. Herein, we reported a facial and robust approach, based on seed-mediated growth and cation exchange, to synthesize $AgInS_2$ NWs, which could be self-assembled into a fingerprint-like structure. The presence of In-S as molecular metal chalcogenide complexes was found to play a key role in the formation and self-assembly of $AgInS_2$ NWs.

The $AgInS_2$ NWs were synthesized by using a seeded-mediated growth method, in which the In precursor solution was quickly injected into the Ag_2S NCs solution. Different aliquots were extracted from the reaction system at different reaction temperatures and time to study the evolution of the morphology, crystal structure and the optical properties. Moreover, the effects of types of In precursors and the usage of 1-dodecanethiol (DDT) on the morphology of the samples were studied to probe the formation mechanism of the self-assembly nanostructures with fingerprint-like shape.

Scheme 1 illustrates the synthetic approach for the growth and self-assembly of $AgInS_2$ NWs. In the first step, Ag_2S NCs as seeds were prepared *via* a thermolysis method. Then, excessive amount of In precursor was injected to initiate the growth of ternary $AgInS_2$

* Corresponding author at: Department of Chemistry, School of Science, Beijing JiaoTong University, Beijing, 100044, China.
** Corresponding author.
E-mail addresses: Haihang.Ye@utdallas.edu (H. Ye), awtang@bjtu.edu.cn (A. Tang).

https://doi.org/10.1016/j.cclet.2020.09.050

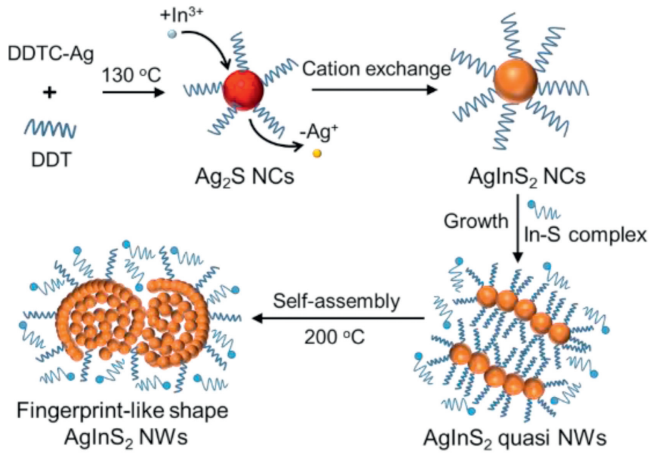

Scheme 1. Schematic illustration showing the morphologies change involved in the synthesis and self-assembly of $AgInS_2$ NCs into quasi NWs and fingerprint-like structures.

NCs through the cation exchange. Further prolonging the reaction and elevating temperature allowed the formation of $AgInS_2$ NWs and InS compounds, and eventually leading to the self-assembly of $AgInS_2$ NWs with fingerprint-like shape. Notably, in the reaction system, no heterogeneous catalysts were required for the NWs growth and the as-obtained products showed a peculiar self-assembly behavior with fingerprint-like shape. By carefully checking the reaction conditions, it was found that the shape of $AgInS_2$ NCs (*e.g.*, NWs) was related to the usage of In precursors and DDT, as well as the reaction thermodynamics.

We started with the preparation of Ag_2S NCs as the initial seeds. In a standard synthesis, a solution of silver diethyldithiocarbamate (Ag-DDTC) in DDT as Ag resource in DDT as the solvent was preheated at 130 °C to form Ag_2S NCs *via* a thermolysis strategy [30]. Then, a DDT solution containing $In(OAc)_3$ and oleic acid (OA) was quickly injected in the seeds solution at 130 °C, the addition of OA can accelerate the dissolution of indium acetate, which was further heated to higher temperature (*e.g.*, 200 or 210 °C) to induce the cation exchange between the In^{3+} and Ag_2S NCs for the formation of ternary $AgInS_2$ NCs. Shortly after the reaction reached the desired temperature, the reaction was discontinued by removing the heating source. Fig. 1a shows a typical transmission

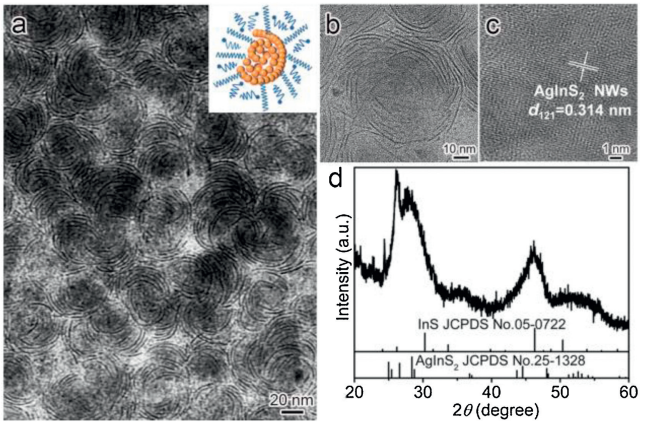

Fig. 1. Morphology and crystal phase characterization of the $AgInS_2$ NWs. (a) Typical TEM image showing the fingerprint-like shape and good uniformity of the products. Inset shows the corresponding model. (b) TEM image of individual fingerprint-like structure at higher magnification. (c) HRTEM image of individual $AgInS_2$ NWs orientated along (121) direction. (d) The corresponding XRD pattern of the product.

electron microscopy (TEM) image of the as-obtained products in 200 °C. It can be seen that the products possess fingerprint-like structures with good uniformity. A TEM image was taken at higher magnification shown in Fig. 1b clearly demonstrates that the fingerprint-like structures were indeed the self-assembly of $AgInS_2$ NWs. As shown in Fig. 1b, the width and length of NWs in 200 °C were roughly 1.2 ± 0.2 nm and 24.0 ± 3.7 nm, respectively (Fig. S1 in Supporting information). The high-resolution TEM (HRTEM) image in Fig. S2 (Supporting information) clearly shows the curly nanowires, indicating that they were alloyed structures, instead of heterostructures (*e.g.*, Ag_2S-$AgInS_2$ or In_2S_3-$AgInS_2$). Fig. 1c shows clearly lattice spacing of the sample, measured as 0.314 nm, which corresponds to the (121) plane of orthorhombic $AgInS_2$. The X-ray diffraction (XRD) pattern shown in Fig. 1d reveals that the products were composed of two phases, in which one could be indexed to the $AgInS_2$ (JCPDS No. 25-1328) and the other was nonstoichiometric InS (JCPDS No. 05-0722) with a distinctive peak around $2\theta = 46°$. We hypothesized that the nonstoichiometric InS species were the molecular metal chalcogenide complex in the format of In-DDT containing InS species, because 1) the stoichiometry of InS does not match the elemental valence; and 2) InS species does not appear neither in the solution nor attach to the NWs as individual NCs as shown in the final products. Interestingly, these compounds played a key role in the formation and self-assembly of $AgInS_2$ NWs, which will be discussed later. Moreover, the energy-dispersive spectroscopy (EDS) elemental mapping images are performed to demonstrate the element distribution. As shown in Fig. S3 (Supporting information) that the Ag, In and S elements are uniformly distributed in the samples.

We first studied the impacts of the reaction thermodynamics on the formation of products, in order to understand the growth mechanism of $AgInS_2$ NWs and their self-assembly behavior. Aliquots extracted from the reaction system at 180 °C after the injection of In precursors with different reaction time (*i.e.*, 10, 15, 25 and 30 min) were characterized. It should be pointed out that under higher reaction temperature, the morphological change was too fast to be monitored and thus low temperature (*i.e.*, 180 °C) was chosen for the examination. The morphological and structural change was shown in Fig. 2. As seen from the TEM images in Fig. 2a and b, at early stage of the reaction (*i.e.*, 10 and 15 min) the products were mainly composed of small NCs with dot-like shape, and only few fingerprint structures were observed. The XRD pattern of the corresponding sample reveals that the product was mainly made of $AgInS_2$ NCs (Fig. 2e). This indicates that the cation exchange between the Ag_2S NCs and In^{3+} ions could take place and complete rapidly, which is in agreement with previous publications [30]. Prolonging the reaction time to 25 and 30 min (Figs. 2c and d, respectively), $AgInS_2$ NWs were formed and self-assembled into fingerprint-like structures, which were dominated in the products. Such morphological evolution was accompanied with the crystal phase change. As seen from the XRD pattern of final product (Fig. 2e), the peak at $2\theta = 46°$ showed up, indicating the presence of InS complex. Thus, the product component consisted of $AgInS_2$ and InS species, which was consistent with the products obtained at higher temperature. Based on the shape evolution during synthesis, we envision that the presence of InS complex played an important role in controlling the shape of the products (*i.e.*, NWs), which further directed their self-assembly behavior.

To further validate the aforementioned argument, we examined the effects of the reaction temperature on the products with the same reaction time (*i.e.*, 10 min). Figs. 3a-c show the TEM images of samples obtained from 210, 200 and 180 °C, and the obvious fingerprint-like structures are observed at 210 and 200 °C, but only small NCs are observed at 180 °C for 10 min. The corresponding XRD patterns reveal a distinctive peak for InS compounds at 200 °C and 210 °C (Fig. 3d), while at lower temperature (180 °C), such a

peak is not observed. Apparently, increasing the reaction temperature accelerates the formation of InS species and thus favoring for the formation of fingerprint-like $AgInS_2$ NWs. In contrast, when none or insufficient amount of InS compounds were present in the reaction system, the $AgInS_2$ NWs could not form and so as the self-assemble structures. It also implies that the formation of fingerprint-like structure is influenced by thermodynamic factors. We further studied the effect of temperature on the formation of $AgInS_2$ NWs. Conducting the same reaction at 170 °C resulted in the formation of dot-like NCs in despite of the reaction time (Fig. S4 in Supporting information). Notably, in this case, the InS species was presented in the reaction system, as seen from the XRD pattern of sample obtained at 60 min. Therefore, the reaction thermodynamics (*i.e.*, high temperature) is also necessary to induce the growth and self-assembly of $AgInS_2$ NWs by providing sufficient energy.

Collectively, the growth and self-assembly of $AgInS_2$ NWs was achieved by the following issues: 1) the presence of InS species, serving as inorganic ligands that directs the morphological evolution and assembling behavior of products; and 2) the reaction thermodynamics that promotes this structural change [31]. Importantly, the optical properties of the products were changed due to the formation of fingerprint-like $AgInS_2$ NWs. The absorption and photoluminescent (PL) spectra were shown in Fig. S5 (Supporting information). A slightly blue-shift was observed in both of the absorption band edge and PL emission maximum as the temperature increased. In other words, when the size of the $AgInS_2$ nanoparticles changed, the absorption band edge showed a slightly blue shift. The corresponding optical band gap is shown in Fig. S6 (Supporting information), the optical band gap can be estimated to be about 2.95–3.05 eV, which is larger than the band gap of bulk orthorhombic $AgInS_2$ (1.98 eV). PL emission spectra can be divided into two peaks, one of the peaks is significantly near 600 nm and the other is near 670 nm, which may attributed to the presence of surface and internal defect states [30].

We then performed the high-resolution X-ray photoelectron spectroscopy (XPS) to analyze the products obtained at different temperature for the Ag, In and S elements (Fig. S7 in Supporting information). For the sake of comparison, the products are marked with *i-iv*. It should be noted that among these four products, only sample *i* was composed of $AgInS_2$ with dot-like shape, while others are the combination of $AgInS_2$ NWs and InS species as evidenced by the TEM images and XRD patterns. The XPS spectrum of Ag 3d region shown in Fig. S7a reveals that the sample *i* displayed two peaks located at 368.1 and 374.1 eV, matching well with the values of Ag $3d_{5/2}$ and Ag $3d_{3/2}$, respectively. Both peaks shift to lower binding energies for the sample *ii-iv*, which may result from the In-S species on the surface of $AgInS_2$ NWs. The ratio of [In]/([Ag]+[In]) quantified from the XPS data was estimated to be 0.63, 0.70, 0.76 and 0.75 for sample *i-iv*, receptively, which further demonstrated that increasing the reaction temperature or prolonging the reaction time at low temperature favors for the formation of InS species. Since these compounds are a type of electron-deficient structures, their adsorption would lead to the enrichment of electrons on the surface of $AgInS_2$ NWs. The binding energy of constituent element would decrease when it adsorbs electrons and *vice versa* [32]. Therefore, the formation and adsorption of InS species lead to the decrease of binding energy in terms of Ag in the products [33]. Similar results are observed in the In element as shown in Fig. S7b, which also arise from the presence of InS species. In addition, the XPS spectra of S 2p peak shown in Fig. S7c, which could be fitted to two different doublet peaks using a spin-orbit splitting of 1.2 eV, indicated the presence of two different sulfur species in the samples. The peak at lower binding energy could be ascribed to sulfide ions of NCs, while the other peaks at higher binding energy were associated with the thiol bonds on the NCs surface [30,34,35]. The slightly shifting of the latter peaks might be attributed to the formation of In-DDT compounds in format of In-thiol bonds. Moreover, the Fourier transform infrared (FTIR) spectra shown in Fig. S8 (Supporting information) demonstrate that the sample obtained at 200 °C exhibit the characteristic peaks from In-DDT complex, further suggesting that the formation of InS species contributed mainly to the self-assembly of NWs.

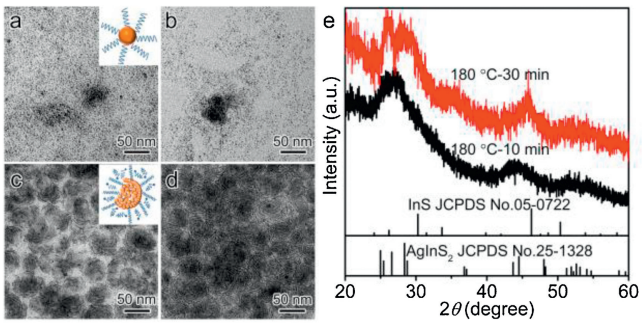

Fig. 2. Temporal-evolution of morphology for the products obtained at 180 °C in a standard synthesis. TEM images of the aliquots extracted at different stages: (a) 10 min; (b) 15 min; (c) 25 min, and (d) 30 min, respectively. (e) XRD patterns of samples obtained at 10 min (black) and 30 min (red), respectively.

We found that the shape of product was dependent on the amount and types of In precursors. Altering the amount of $In(OAc)_3$ with In/Ag ratio of 1:2 and 1:1, while kept other conditions the same as in a standard synthesis, produced different shapes of products as shown in Figs. S9a and b (Supporting information), respectively. Clearly, decreasing the amount of $In(OAc)_3$ affected the morphology of the products dramatically. In the Ag-rich case (In/Ag = 1:2, Fig. S9a), the product exhibited hybrid shapes. The black dots adsorbed on surface and dispersed individually could be Ag_2S NCs, while the knife-like particles could be $AgInS_2$ NCs and the rest might be Ag_2S-$AgInS_2$ heteronanostructures [30,36]. When the In/Ag was set to be 1:1 (Fig. S9b), most of the monodispersed dots disappeared and the products remained as triangular NCs with dark "head" and bright "tail". Such a head-tail shape of the NCs could be classified as a type of heteronanostructures. Also, the black dots were much less than those in the Ag-rich case, due to the increasing amount of In precursor (more Ag_2S turned into $AgInS_2$). These results were in consistent with the XRD patterns shown in the Fig. S10 (Supporting information), where the Ag_2S peaks around $2\theta = 35°$ gradually disappeared when the amount of $In(OAc)_3$ increases. Notably, in those cases, none of the peaks represented for InS species appeared and thus neither $AgInS_2$ NWs nor self-assembly were observed. In contrast, further increasing the In/Ag ratio to 3:1 resulted in fingerprint-like $AgInS_2$ NWs (Fig. 1a). Taken together, those results strongly support our hypothesis that the InS complex was the key to the formation and self-assembly of $AgInS_2$ NWs. In addition, changing the types of In precursors has significant effects on the morphologies of products. TEM images of $AgInS_2$ NCs obtained by using of $In(acac)_3$ and $InCl_3$ are shown in Figs. S9c and d (Supporting information), respectively. Such a difference might be induced by the different binding energy of In-DDT compounds and additional anions presented in the reaction system.

Lastly, the dose effects of capping ligands (DDT) on products were also studied. In many cases, the capping ligands are involved in the growth of colloidal NCs, during which they are adsorbed on the NCs' surfaces [30]. Therefore, they not only prevent NCs from aggregation, but also direct morphological evolution of growing NCs. In the present study, when only 2 mL of DDT was used in the reaction system, the products possess a similar shape as the Ag_2S-$AgInS_2$ heteronanostructures (Fig. S11a in Supporting information). It was similar to the case shown in Fig. S9a. Further

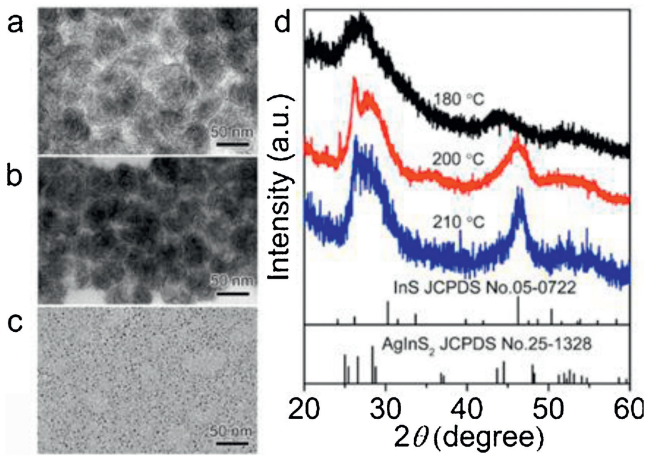

Fig. 3. TEM images of $AgInS_2$ NCs at different temperatures for 10 min: (a) 210 °C; (b) 200 °C; (c) 180 °C. (d) The corresponding XRD patterns.

increasing the DDT dose to 4 and 6 mL leads to the formation of $AgInS_2$ NCs and NWs, and the corresponding TEM images were provided in Figs. S11b and c (Supporting information), respectively. In Fig. S11b (Supporting information), dot-like $AgInS_2$ NCs were appeared with the co-existence of small portion of $AgInS_2$ NWs. Nevertheless, self-assembly structures of $AgInS_2$ NWs started dominating when sufficient amount of DDT was used (*e.g.*, 6 mL), where dot-like NCs could still be observed. Further increasing the DDT amount to 12 mL produced uniform fingerprint-like structures as obtained from a standard synthesis (Fig. 1a).

In summary, we have demonstrated a facile method based on the seeded growth and cation exchange strategy for the synthesis and self-assembly of $AgInS_2$ NWs with fingerprint-like shape. The key was to direct the formation of InS complex to induce the growth of NWs and thus self-assembly behavior by controlling multiple factors including the reaction kinetics, amount and type of In precursor, and DDT usage. Significantly, this study not only provides the first successful attempt for the synthesis of high-quality $AgInS_2$ NWs, but also provides a simple yet efficient route to controllable self-assembly structures. We believe the synthetic strategy reported here can also be extended to the synthesis of NWs of other chalcogenide semiconductors and the development of self-assemble nanostructures with unusual properties.

Declaration of competing interest

The authors declare no conflict of interest.

Acknowledgments

This work was supported by the National Natural Science Foundation of China (Nos. 61735004 and 61974009). The author appreciates the Key Laboratory of New Energy and Rare Earth Resource Utilization of State Ethnic Affairs Commission (No. NERE201903).

References

[1] T. Torimoto, T. Adachi, K. Okazaki, et al., J. Am. Chem. Soc. 129 (2007) 12388–12389.
[2] Y. Hamanaka, T. Ogawa, M. Tsuzuki, T. Kuzuya, J. Phys. Chem. C 115 (2011) 17861792.
[3] Y. Hamanaka, T. Ogawa, M. Tsuzuki, K. Ozawa, T. Kuzuya, J. Lumin. 133 (2013) 121–124.
[4] C.Q. Cai, L.L. Zhai, Y.H. Ma, et al., J. Power. Source 341 (2017) 11–18.
[5] M. Jagadeeswararao, A. Swarnkar, G.B. Markad, A. Nag, J. Phys. Chem. C 120 (2016) 19461–19469.
[6] A. Guchhait, A.J. Pal, ACS Appl. Mater. Interfaces 5 (2013) 4181–4189.
[7] D.B. Choi, S. Kim, H.C. Yoon, et al., J. Mater. Chem. C 5 (2017) 953–959.
[8] C. Ji, M. Lu, H. Wu, et al., ACS Appl. Mater. Interfaces 9 (2017) 8187–8193.
[9] X.J. Kang, Y.C. Yang, L. Wang, S. Wei, D.C. Pan, ACS Appl. Mater. Interfaces 7 (2015) 27713–27719.
[10] M. Ko, H.C. Yoon, H. Yoo, et al., Adv. Funct. Mater. 27 (2017) 1602638.
[11] W.J. Zhang, C.Y. Pan, F. Cao, H.R. Wang, X.Y. Yang, J. Mater. Chem. C 6 (2018) 10233–10240.
[12] H.T. Ma, L.J. Pan, J. Wang, L. Zhang, Z.L. Zhang, Chin. Chem. Lett. 30 (2019) 79–82.
[13] L. Wang, X.J. Kang, D.C. Pan, Inorg. Chem. 56 (2017) 6122–6130.
[14] R.X. Han, J.R. Peng, Y. Xiao, et al., Chin. Chem. Lett. 31 (2020) 1717–1728.
[15] M.D. Regulacio, K.Y. Win, S.L. Lo, et al., Nanoscale 5 (2013) 2322–2327.
[16] D.W. Deng, L.Z. Qu, Y.Q. Gu, J. Mater. Chem. C 2 (2014) 7077–7085.
[17] Z.S. Luo, H. Zhang, J. Huang, X.H. Zhong, J. Colloid Interface Sci. 377 (2012) 27–33.
[18] I. Tsuji, H. Kato, A. Kudo, Chem. Mater. 18 (2006) 1969–1975.
[19] T. Chevallier, G.L. Blevennec, F. Chandezon, Nanoscale 8 (2016) 7612–7620.
[20] H.Z. Zhong, Z.L. Bai, B.S. Zou, J. Phys. Chem. Lett. 3 (2012) 3167–3175.
[21] B. Cichy, D. Wawrzynczyk, M. Samoc, W. Strek, J. Mater. Chem. C 5 (2017) 149–158.
[22] H. Doh, S. Hwang, S. Kim, Chem. Mater. 28 (2016) 8123–8127.
[23] X. Wang, C.P. Xie, J.S. Zhong, X.J. Liang, W.D. Xiang, J. Alloys Compd. 648 (2015) 127–133.
[24] Q. Li, C. Zou, L.L. Zhai, et al., CrystEngComm. 15 (2013) 1806–1813.
[25] C. Zou, M. Li, L.J. Zhang, et al., CrystEngComm. 13 (2011) 3515–3520.
[26] A.W. Tang, S.C. Qu, K. Li, et al., Nanotechnology 21 (2010) 285602.
[27] A.W. Tang, Y. Wang, H.H. Ye, et al., Nanotechnology 24 (2013) 355602.
[28] C.L. Poyser, T. Czerniuk, A. Akimov, et al., ACS Nano 10 (2016) 1163–1169.
[29] Y. Taniguchi, T. Takishita, T. Kawai, T. Nakashima, Angew. Chem. Int. Ed. 55 (2016) 2083–2086.
[30] B. Zeng, F. Chen, Z.Y. Liu, et al., J. Mater. Chem. C 7 (2019) 1307–1315.
[31] X.M. Li, H.B. Shen, J.Z. Niu, et al., J. Am. Chem. Soc. 132 (2010) 12778–12779.
[32] J.Z. Qin, X. Hu, X.Y. Li, et al., Nano Energy 61 (2019) 27–35.
[33] S. Cingarapu, M.A. Ikenberry, D.B. Hamal, et al., Langmuir 28 (2012) 3569–3575.
[34] Z.Y. Guan, A.W. Tang, P.W. Lv, et al., Adv. Opt. Mater. 6 (2018) 1701389.
[35] O. Stroyuk, A. Raevskaya, F. Spranger, et al., J. Phys. Chem. C 122 (2018) 13648–13658.
[36] F. Huang, J.C. Zhou, J. Xu, Y.S. Wang, Nanoscale 6 (2014) 2340–2344.